Research Article | Vol. 8, No. 9 | 1 Sep 2017 | BIOMEDICAL OPTICS EXPRESS 4243
Biomedical Optics EXPRESS

Quantification of collagen organization in histopathology samples using liquid crystal based polarization microscopy

ADIB KEIKHOSRAVI,[1,2,3,7] YUMING LIU,[1,7] COLE DRIFKA,[1,2,3] KAITLIN M. WOO,[6] AMITABH VERMA,[4] RUDOLF OLDENBOURG,[4,5] AND KEVIN W. ELICEIRI[1,2,3,*]

[1]*Laboratory for Optical and Computational Instrumentation, University of Wisconsin at Madison, Madison WI, USA*
[2]*Biomedical Engineering Department, University of Wisconsin at Madison, Madison WI, USA*
[3]*Morgridge Institute for Research, Madison WI, USA*
[4]*Marine Biological Laboratory, Woods Hole, MA, USA*
[5]*Department of Physics, Brown University, Providence, RI, USA*
[6]*Department of Biostatistics and Medical informatics, Brown University, Providence, RI, USA*
[7]*These authors have contributed equally*
[*]*eliceiri@wisc.edu*

Abstract: A number of histopathology studies have utilized the label free microscopy method of Second Harmonic Generation (SHG) to investigate collagen organization in disease onset and progression. Here we explored an alternative label free imaging approach, LC-PolScope that is based on liquid crystal based polarized light imaging. We demonstrated that this more accessible technology has the ability to visualize all fibers of interest and has a good to excellent correlation between SHG and LC-PolScope measurements in fibrillar collagen orientation and alignment. This study supports that LC-PolScope is a viable alternative to SHG for label free collagen organization measurements in thin histology sections.

OCIS codes: (110.0180) Microscopy; (100.2960) Image analysis; (190.2620) Harmonic generation and mixing; (260.5430) Polarization; (110.1758) Computational imaging.

References and links

1. B.-M. Kim, J. Eichler, K. M. Reiser, A. M. Rubenchik, and L. B. Da Silva, "Collagen structure and nonlinear susceptibility: Effects of heat, glycation, and enzymatic cleavage on second harmonic signal intensity," Lasers Surg. Med. **27**(4), 329–335 (2000).
2. M. B. Lilledahl, O. A. Haugen, C. de Lange Davies, and L. O. Svaasand, "Characterization of vulnerable plaques by multiphoton microscopy," J. Biomed. Opt. **12**(4), 044005 (2007).
3. P. Odetti, M. A. Pronzato, G. Noberasco, L. Cosso, N. Traverso, D. Cottalasso, and U. M. Marinari, "Relationships between glycation and oxidation related fluorescences in rat collagen during aging. An in vivo and in vitro study," Lab. Invest. **70**(1), 61–67 (1994).
4. S. Tanaka, G. Avigad, B. Brodsky, and E. F. Eikenberry, "Glycation induces expansion of the molecular packing of collagen," J. Mol. Biol. **203**(2), 495–505 (1988).
5. W. Sun, S. Chang, D. C. S. Tai, N. Tan, G. Xiao, H. Tang, and H. Yu, "Nonlinear optical microscopy: use of second harmonic generation and two-photon microscopy for automated quantitative liver fibrosis studies," J. Biomed. Opt. **13**(6), 064010 (2008).
6. T. T. Le, I. M. Langohr, M. J. Locker, M. Sturek, and J.-X. Cheng, "Label-free molecular imaging of atherosclerotic lesions using multimodal nonlinear optical microscopy," J. Biomed. Opt. **12**(5), 054007 (2007).
7. M. W. Conklin, J. C. Eickhoff, K. M. Riching, C. A. Pehlke, K. W. Eliceiri, P. P. Provenzano, A. Friedl, and P. J. Keely, "Aligned collagen is a prognostic signature for survival in human breast carcinoma," Am. J. Pathol. **178**(3), 1221–1232 (2011).
8. C. R. Drifka, J. Tod, A. G. Loeffler, Y. Liu, G. J. Thomas, K. W. Eliceiri, and W. J. Kao, "Periductal stromal collagen topology of pancreatic ductal adenocarcinoma differs from that of normal and chronic pancreatitis," Mod. Pathol. **28**(11), 1470–1480 (2015).
9. O. Nadiarnykh, R. B. LaComb, M. A. Brewer, and P. J. Campagnola, "Alterations of the extracellular matrix in ovarian cancer studied by Second Harmonic Generation imaging microscopy," BMC Cancer **10**(1), 94 (2010).
10. A. Keikhosravi, J. S. Bredfeldt, A. K. Sagar, and K. W. Eliceiri, "Second-harmonic generation imaging of cancer," Methods Cell Biol. **123**, 531–546 (2014).

#297374 https://doi.org/10.1364/BOE.8.004243
Journal © 2017 Received 8 Jun 2017; revised 11 Aug 2017; accepted 23 Aug 2017; published 29 Aug 2017

Biomedical Optics EXPRESS

11. G. Ayala, J. A. Tuxhorn, T. M. Wheeler, A. Frolov, P. T. Scardino, M. Ohori, M. Wheeler, J. Spitler, and D. R. Rowley, "Reactive stroma as a predictor of biochemical-free recurrence in prostate cancer," Clin. Cancer Res. **9**(13), 4792–4801 (2003).
12. I. Allon, M. Vered, A. Buchner, and D. Dayan, "Stromal differences in salivary gland tumors of a common histopathogenesis but with different biological behavior: a study with picrosirius red and polarizing microscopy," Acta Histochem. **108**(4), 259–264 (2006).
13. P. P. Provenzano, C. Cuevas, A. E. Chang, V. K. Goel, D. D. Von Hoff, and S. R. Hingorani, "Enzymatic targeting of the stroma ablates physical barriers to treatment of pancreatic ductal adenocarcinoma," Cancer Cell **21**(3), 418–429 (2012).
14. P. Arun Gopinathan, G. Kokila, M. Jyothi, C. Ananjan, L. Pradeep, and S. Humaira Nazir, "Study of Collagen Birefringence in Different Grades of Oral Squamous Cell Carcinoma Using Picrosirius Red and Polarized Light Microscopy," Scientifica (Cairo) **2015**, 802980 (2015).
15. B. K. Brisson, E. A. Mauldin, W. Lei, L. K. Vogel, A. M. Power, A. Lo, D. Dopkin, C. Khanna, R. G. Wells, E. Puré, and S. W. Volk, "Type III Collagen Directs Stromal Organization and Limits Metastasis in a Murine Model of Breast Cancer," Am. J. Pathol. **185**(5), 1471–1486 (2015).
16. L. C. Junqueira, G. Bignolas, and R. R. Brentani, "Picrosirius staining plus polarization microscopy, a specific method for collagen detection in tissue sections," Histochem. J. **11**(4), 447–455 (1979).
17. C. R. Drifka, A. G. Loeffler, K. Mathewson, G. Mehta, A. Keikhosravi, Y. Liu, S. Lemancik, W. A. Ricke, S. M. Weber, W. J. Kao, and K. W. Eliceiri, "Comparison of Picrosirius Red Staining With Second Harmonic Generation Imaging for the Quantification of Clinically Relevant Collagen Fiber Features in Histopathology Samples," J. Histochem. Cytochem. **64**(9), 519–529 (2016).
18. X. Chen, O. Nadiarynkh, S. Plotnikov, and P. J. Campagnola, "Second harmonic generation microscopy for quantitative analysis of collagen fibrillar structure," Nat. Protoc. **7**(4), 654–669 (2012).
19. P. J. Campagnola, A. C. Millard, M. Terasaki, P. E. Hoppe, C. J. Malone, and W. A. Mohler, "Three-dimensional high-resolution second-harmonic generation imaging of endogenous structural proteins in biological tissues," Biophys. J. **82**(1), 493–508 (2002).
20. B. D. Quan and E. D. Sone, "Cryo-TEM analysis of collagen fibrillar structure," Methods Enzymol. **532**, 189–205 (2013).
21. M. Plodinec, M. Loparic, C. A. Monnier, E. C. Obermann, R. Zanetti-Dallenbach, P. Oertle, J. T. Hyotyla, U. Aebi, M. Bentires-Alj, R. Y. H. Lim, and C.-A. Schoenenberger, "The nanomechanical signature of breast cancer," Nat. Nanotechnol. **7**(11), 757–765 (2012).
22. M. Kobayashi, Y. Furuya, T. Okabayashi, and K. Araki, "Scanning electron microscopic study of the three-dimensional structure of the collagen sheath surrounding cancer cells after single high-dose irradiation," Med. Mol. Morphol. **39**(2), 106–112 (2006).
23. K. Burke, P. Tang, and E. Brown, "Second harmonic generation reveals matrix alterations during breast tumor progression," J. Biomed. Opt. **18**(3), 031106 (2012).
24. R. M. Williams, W. R. Zipfel, and W. W. Webb, "Interpreting Second-Harmonic Generation Images of Collagen I Fibrils," Biophys. J. **88**(2), 1377–1386 (2005).
25. C. J. Hanley, F. Noble, M. Ward, M. Bullock, C. Drifka, M. Mellone, A. Manousopoulou, H. E. Johnston, A. Hayden, S. Thirdborough, Y. Liu, D. M. Smith, T. Mellows, W. J. Kao, S. D. Garbis, A. Mirnezami, T. J. Underwood, K. W. Eliceiri, and G. J. Thomas, "A subset of myofibroblastic cancer-associated fibroblasts regulate collagen fiber elongation, which is prognostic in multiple cancers," Oncotarget **7**(5), 6159–6174 (2016).
26. J. S. Bredfeldt, Y. Liu, M. W. Conklin, P. J. Keely, T. R. Mackie, and K. W. Eliceiri, "Automated quantification of aligned collagen for human breast carcinoma prognosis," J. Pathol. Inform. **5**(1), 28 (2014).
27. R. D. Allen, J. Brault, and R. D. Moore, "A new method of polarization microscopic analysis I. Scanning with a Birefringence Detection System," J. Cell Biol. **18**(2), 223–235 (1963).
28. S. Inoué and H. Sato, *Molecular Architecture in Cell Physiology* (Prentice-Hall, Englewood, Clifs, NJ, 1966).
29. R. Oldenbourg and G. Mei, "New polarized light microscope with precision universal compensator," J. Microsc. **180**(2), 140–147 (1995).
30. R. Oldenbourg, "A new view on polarization microscopy," Nature **381**(6585), 811–812 (1996).
31. M. Shribak and R. Oldenbourg, "Techniques for fast and sensitive measurements of two-dimensional birefringence distributions," Appl. Opt. **42**(16), 3009–3017 (2003).
32. N. L. Rosin, N. Agabalyan, K. Olsen, G. Martufi, V. Gabriel, J. Biernaskie, and E. S. Di Martino, "Collagen structural alterations contribute to stiffening of tissue after split-thickness skin grafting," Wound Repair Regen. **24**(2), 263–274 (2016).
33. Z. Nong, C. O'Neil, M. Lei, R. Gros, A. Watson, A. Rizkalla, K. Mequanint, S. Li, M. J. Frontini, Q. Feng, and J. G. Pickering, "Type I Collagen Cleavage Is Essential for Effective Fibrotic Repair after Myocardial Infarction," Am. J. Pathol. **179**(5), 2189–2198 (2011).
34. R. Oldenbourg, "Polarization microscopy with the LC-PolScope," in *Live Cell Imaging: A Laboratory Manual.*, R. D. Goldman and D. L. Spector, eds. (Cold Spring Harbor Laboratory Press, 2005).
35. J. Schindelin, I. Arganda-Carreras, E. Frise, V. Kaynig, M. Longair, T. Pietzsch, S. Preibisch, C. Rueden, S. Saalfeld, B. Schmid, J.-Y. Tinevez, D. J. White, V. Hartenstein, K. Eliceiri, P. Tomancak, and A. Cardona, "Fiji: an Open-Source platform for biological-image analysis," Nat. Methods **9**(7), 676–682 (2012).
36. S. Saalfeld, A. Cardona, V. Hartenstein, and P. Tomančák, "As-rigid-as-possible mosaicking and serial section registration of large ssTEM datasets," Bioinformatics **26**(12), i57–i63 (2010).

Biomedical Optics EXPRESS

37. J. S. Bredfeldt, Y. Liu, C. A. Pehlke, M. W. Conklin, J. M. Szulczewski, D. R. Inman, P. J. Keely, R. D. Nowak, T. R. Mackie, and K. W. Eliceiri, "Computational segmentation of collagen fibers from second-harmonic generation images of breast cancer," J. Biomed. Opt. **19**(1), 016007 (2014).
38. P. Berens, "CircStat: A MATLAB Toolbox for Circular Statistics," J. Stat. Softw. **31**(10), 21 (2009).
39. A. Hamlett, L. Ryan, P. Serrano-Trespalacios, and R. Wolfinger, "Mixed Models for Assessing Correlation in the Presence of Replication," J. Air Waste Manag. Assoc. **53**(4), 442–450 (2003).
40. D. V. Cicchetti, "Guidelines, criteria, and rules of thumb for evaluating normed and standardized assessment instruments in psychology," Psychol. Assess. **6**(4), 284–290 (1994).
41. D. G. Altman and J. M. Bland, "Measurement in Medicine: The Analysis of Method Comparison Studies," J. R. Stat. Soc. Ser. Stat. **32**, 307–317 (1983).
42. B. C. Vidal, M. L. Mello, and E. R. Pimentel, "Polarization microscopy and microspectrophotometry of Sirius Red, Picrosirius and Chlorantine Fast Red aggregates and of their complexes with collagen," Histochem. J. **14**(6), 857–878 (1982).
43. D. B. Murphy and M. W. Davidson, *Fundamentals of Light Microscopy and Electronic Imaging* (John Wiley & Sons, 2012).
44. C. J. Cicchetti and J. A. Dubin, "A Microeconometric Analysis of Risk Aversion and the Decision to Self-Insure," J. Polit. Econ. **102**(1), 169–186 (1994).

1. Introduction

Collagen, the most abundant protein in vertebrates, forms the structural network of the extracellular matrix (ECM) in biological tissues. Different collagen types may exhibit different structural characteristics. For example, fibrillar collagen type I is composed of triple-helical macromolecules that self-assemble into fibrils and fibers. The amount, distribution, and structural organization of fibrillar collagen are all important factors underlying the properties of tissues and play an integral role in many diseases including cancer. There have been many studies using collagen as a biomarker in wound healing, aging, and other pathologies including fibrosis, atherosclerosis and diabetes [1–6]. Collagen organization parameters, specifically fiber orientation and alignment, have been shown repeatedly to play an important role in progression and metastasis of cancer [7–10].

A variety of established methods currently exist to visualize collagen fibers in tissue. Some of these methods are only applicable in thin-sectioned histological samples such as 1) Stains: picrosirius red (PSR), Movat's pentachrome and Masson's trichrome [11–14]; 2) Antibody detection [15]; 3) Polarized microscopy, which is usually used to enhance the visualization of PSR stained tissue [16,17]; 4) SHG imaging [18,19]. Other methods to visualize collagen such as electron microscopy [20], atomic force microscopy [21], and scanning electron microscopy [22] have largely been limited to non-routine highly specialized application due to a very small field of view, highly technical sample preparation, and very high cost equipment.

The non-centrosymmetric structure of fibrillar collagen, which is necessary for producing second harmonic signal, makes SHG highly specific to this molecule [19]. Because of its specificity, resolution, label-free detection, and ability to optically section, SHG has become a very popular fibrillar collagen imaging method. However, high cost, complexity, and the need in some cases for experienced optical engineers make it impractical for routine pathology practices. Undoubtedly, SHG has great advantages in terms of imaging depth and higher-order information using forward to backward ratio [23] and polarization based studies [9,24] etc. However, as most of the reported histopathological studies are only using thin pathology sections with a standard thickness of 5 μm and only looking at collagen topology or organization, the advantages mentioned above are not of primary interest [7,8,25,26].

Polarized light microscopy is capable of non-destructively measuring molecular organization in biological samples in their native conditions. However, traditional polarized microscopes can only image anisotropic structures that have a limited range of orientations with respect to the polarization axes of the microscope. Furthermore, rapid measurements are restricted to a single image point or single area that exhibits uniform birefringence or other forms of optical anisotropy [27]. As a result, it will take an inordinately long time to compare measurements at several image points [28]. To overcome the limitations of the traditional

Biomedical Optics EXPRESS

polarized light microscope, Oldenbourg et al. developed a new type of polarized light microscope, the LC-PolScope, which incorporates a precision universal compensator made of two liquid crystal variable retarders [29–31]. The two variable retarders are computer controlled and replace the traditional compensator of the polarizing microscope. The LC-PolScope is typically implemented on a wide field microscope equipped with CCD camera and specially designed, computerized image analysis system. This LC-PolScope system and its open access implementation OpenPolScope (openpolscope.org) can provide fast measurements of specimen anisotropy, such as retardance and slow axis orientation, at all points of the image constituting the field of view. Because of its fast speed, high sensitivity, and ease of use for measurements of optical anisotropies, the LC-PolScope can advance the analytical power of the polarizing microscope in all of its traditional application areas such as biology, physics and material science (Oldenbourg, R. (2005) Polarization microscopy with the LC-PolScope. in R. D. Goldman and D. L. Spector (eds.) *Live Cell Imaging: A Laboratory Manual*. Cold Spring Harbor, NY: Cold Spring Harbor Laboratory Press. http://hdl.handle.net/1912/6277). We report here the first use of the birefringence mode of the LC-PolScope for quantitatively imaging fibrillar collagen in tissues, and comparing it against SHG microscopy. Previous studies [32,33] have used the LC-PolScope as a tool for looking at directionality of collagen fibers and alignment in collagen gels but not for quantitating collagen organization in pathology samples. This study proposes that the LC-PolScope could be a powerful tool for histopathology by measuring changes in collagen organization. Images from both, PolScope and SHG imaging were quantitatively compared using breast and pancreatic cancer pathology slides. The estimated correlation between orientation data measured by SHG and PolScope was 0.68 for breast cancer, and 0.80 for pancreatic cancer, and the estimated correlation for alignment was 0.69 in breast cancer and 0.65 for pancreatic cancer. Our investigation shows that the LC-PolScope, a cheaper, and simpler modality than SHG, can be used for the quantification of collagen fibers orientation and alignment.

2. Methods

2.1 Imaging systems

SHG imaging was performed using a custom-built multiphoton microscope (CAMM) at the Laboratory for Optical and Computational Instrumentation (LOCI) at the University of Wisconsin-Madison. This system was used to collect bright field images as well as forward direction SHG excited by a MIRA 900 Ti: Sapphire laser (Coherent, Santa Clara, CA) tuned to 780 nm and 100fs pulse length. A circularly polarized laser beam was generated and focused on the sample using a 40X`/1.25NA water immersion objective (Nikon, Melville, NY). The forward SHG signal was separated using a 390/18 nm filter (ThorLabs) and sent to a H7422-40P GaAsP photomultiplier tube (Hamamatsu, Hamamatsu, Japan). The imaging system and the motorized stage were controlled by in house developed acquisition software, WiscScan (http://loci.wisc.edu/software/wiscscan).

The LC-PolScope was implemented using the OpenPolScope hardware and software for birefringence imaging (openpolscope.org), and built around a Nikon Eclipse TE200 equipped with a 549/15 nm interference filter, 20x/0.4NA Plan objective and dry condenser (0.85 NA). Images were acquired using an ORCA-Flash4.0 V2 Digital CMOS camera (Hamamatsu, Hamamatsu, Japan).

Polarized picrosirius imaging was performed on a traditional transmission pathology microscope (BX53; Olympus Corp.) using a 20 × objective (UPlanFL N NA = 0.50; Olympus Corp.) without polarizers (PSR) and with linear polarizers (PSR-POL). Images were digitally captured using cellSens acquisition platform (Olympus Corp.).

Biomedical Optics EXPRESS

2.2 Sample preparation

As a positive control for collagen signal, collagen type I, formalin fixed paraffin embedded (FFPE) human colon tissue was commercially obtained (BioServe Biotechnologies, Beltsville, MD). Tissue sections were cut at 5 µm, mounted on slides, and stained with anti-collagen I antibody (Abcam, rabbit monoclonal, clone EPR7785). Human pancreatic tumor tissues were obtained either as FFPE tissue blocks from our institution (UW IRB # 2013-0148) or as a tissue microarray from a commercial vendor (US Biomax, #HPan-Ade180Sur-01). All pancreatic tissues were sectioned and stained with hematoxylin and eosin (H&E) per standard procedures and three adjacent sections to H&E stained samples were used for picrosirius red staining. Human breast tissues were obtained either as formalin fixed tissue blocks from our institution that we paraffin embedded, sectioned at 5 µm, mounted on slides, and stained with hematoxylin and eosin (H&E) per standard procedures. We also used a tissue microarray of breast cancer patients from previous studies [7,26].

2.3 LC-PolScope system

The design of the LC-PolScope for birefringence imaging is similar to that of the traditional polarized light microscope except for two major modifications: 1) the specimen is illuminated with near circular polarized light; and 2) the traditional compensator is replaced by a liquid crystal based universal compensator. To 1), in a traditional polarized light microscope, the specimen is illuminated with linearly polarized light, in which case the images display only those anisotropic structures that have a limited range of orientations with respect to the polarization axes of the microscope. In the LC-PolScope, however, a circular analyzer and a controllable circular/elliptical polarizer, enable the instrument to detect all the fibers in all directions with very high sensitivity, even without any staining. To 2), in the LC-PolScope, the traditional crystal compensator is replaced with a set of two liquid crystal variable retarders. The two liquid crystal devices are controlled electronically by a computer and can rapidly produce any polarization state. The schematic diagram of the birefringence LC-PolScope is illustrated in Fig. 1 [34].

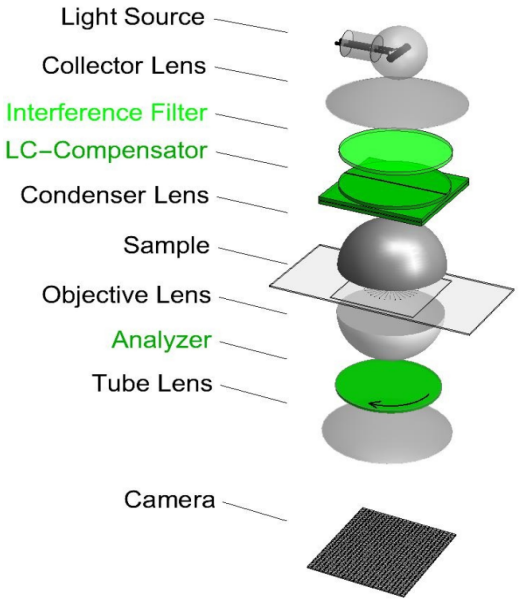

Fig. 1. Schematic diagram of the birefringence LC-PolScope.

Biomedical Optics EXPRESS

To obtain a birefringence image that represents the retardance and slow axis orientation in every image point, the system takes five images at five different polarization states. The first polarization setting produces circularly polarized light, and the other four settings produce elliptically polarized light with different long axis orientations. The 5 raw images are then used to generate high resolution maps of specimen retardance and slow axis orientation using image arithmetic previously described by [31].

2.4 Image analysis

Collagen organization parameters, specifically fiber orientation and alignment, have been shown repeatedly to play an important role in progression and metastasis of cancer [7–10]. Since these studies mostly use SHG for collagen imaging, we used the following workflow to show the alignment and orientation are easily measurable using the LC-Polscope, which are in agreement with the results from SHG imaging: (1) SHG and PolScope images were manually registered with the image analysis package Fiji [35] using landmark correspondences plugin [36], to find the best affine transform; (2) All the images were analyzed using the analysis program CT-FIRE [37] to extract all the individual fibers; and (3) To calculate the alignment and orientation, CurveAlign [26], another custom built fiber network analysis software developed at LOCI was used in CT-FIRE fiber segments mode. In step (2), before CT-FIRE analysis, the PolScope images were converted from 16-bit to 8-bit and a threshold of 25 was applied to 7 breast cancer samples to remove the background and very low birefringent molecules such as cell membrane for a better visualization; in CT-FIRE analysis, background threshold was set to 3-6 for SHG images and thresholded PolScope images, and 30-40 for other PolScope images. For the thresholded PolScope images, we did not change the image look up table of the original images whose CT-FIRE threshold would be a simple addition of two corresponding thresholds mentioned above. In step (3), to account for the difference in collagen content and find the representative collagen patterns in the images, 2-4 regions of interest (ROIs) with different sizes (256 pixels x256 pixels, 512 pixels x 512 pixels, 1024 pixels x 1024 pixels) were manually annotated using ROI manager of CurveAlign for the registered SHG-PolScope images, and the orientation and alignment of fibers within each ROI were calculated.

Fiber orientation was defined as the angle with respect to the horizontal axis, ranging from 0° to 180°. To overcome the angle ambiguity between the angles around lower limit and upper limit, e.g., 0° and 180° essentially indicate the same orientation but the difference in absolute angle is significant, we used a sinusoid function "$\sin(\frac{\pi * x}{180})$" to map the orientation values from 0 to 180 degrees to the [0, 1], where x is the orientation value in degree. Collagen alignment is a measure of the similarity of the orientations of collagen fibers in a defined area, calculated as the mean resultant vector length in circular statistics [38]. The alignment coefficient ranged from 0.0 to 1.0, where larger alignment coefficients indicates fibers in a given image or ROI are more aligned.

2.5 Statistical analysis

Correlation assessment was conducted on each of the fiber metrics(fiber orientation and alignment), measured by PolScope and SHG, by using a linear mixed-effects model with unstructured covariance matrix (for both the random effects and random error) in SAS 9.4 to account for the repeated measures per patient [39]. The correlation value ranges from −1 to + 1, where values of + 1 or −1 denote perfect concordance and discordance, while a value of zero denotes its complete absence. The guidelines for interpretation from [40] are as follows: less than 0.40 - poor; 0.40-0.59 fair; 0.60-0.74 good; 0.75-1.00 excellent.

Biomedical Optics EXPRESS

3. Results

The first step for assessing LC-PolScope as a collagen imaging tool was to verify its ability to visualize fibrillar collagen type I. To this end, we performed collagen I antibody staining on colon tissue, which provides a positive control as collagen I is robustly expressed surrounding intestinal crypts. Figure 2 shows two image samples of the collagen I antibody stained colon tissue. In this figure each row shows a different field of view on tissue slide. The images on the right column are the bright field images of the antibody stained tissue and on the left column the PolScope images (red channel) are overlaid on the bright field images. The brown fibrillar structure in the right column is collagen type I fibers. Through a visual inspection, all fibers stained with collagen type I antibody were also observed in PolScope images. Since PolScope is able to visualize birefringent materials, we can also see cell bilipid membranes, although they were much dimmer than collagen.

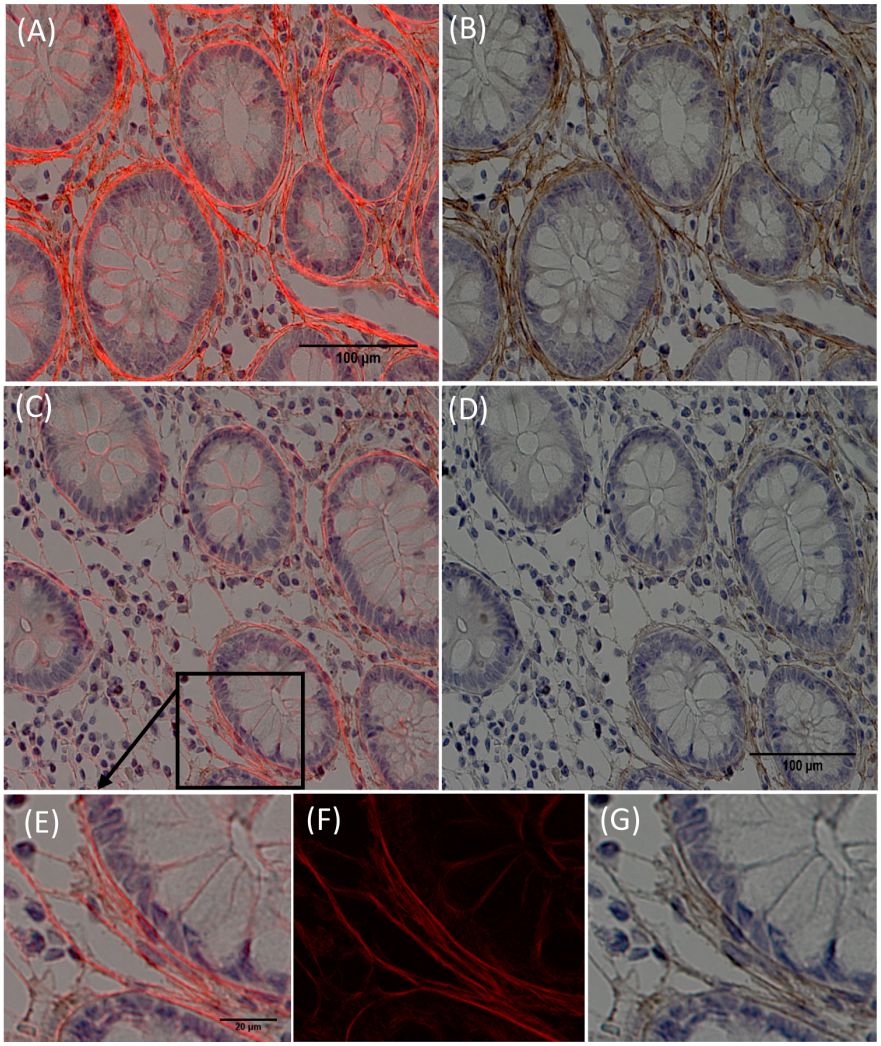

Fig. 2. PolScope can detect all collagen fibers of colon tissue stained with collagen type I antibody. Collagen type I antibody stained colon tissue sample imaged with bright field (B), (D), PolScope in red channel overlaid on bright field (A), (C). The bottom row shows a closer view of the collagen fibers imaged with PolScope overlaid on bright field (E), PolScope image (F) and the bright field image (G).

Biomedical Optics EXPRESS

Figure 3 compares collagen imaging using PolScope (A) and traditional polarized microscope (B) of a pancreatic cancer tissue slide. The bright field image is shown in part (C). Besides orientation independency of the PolScope, it can also visualize thinner fibers, which are not visible using traditional polarized microscopy.

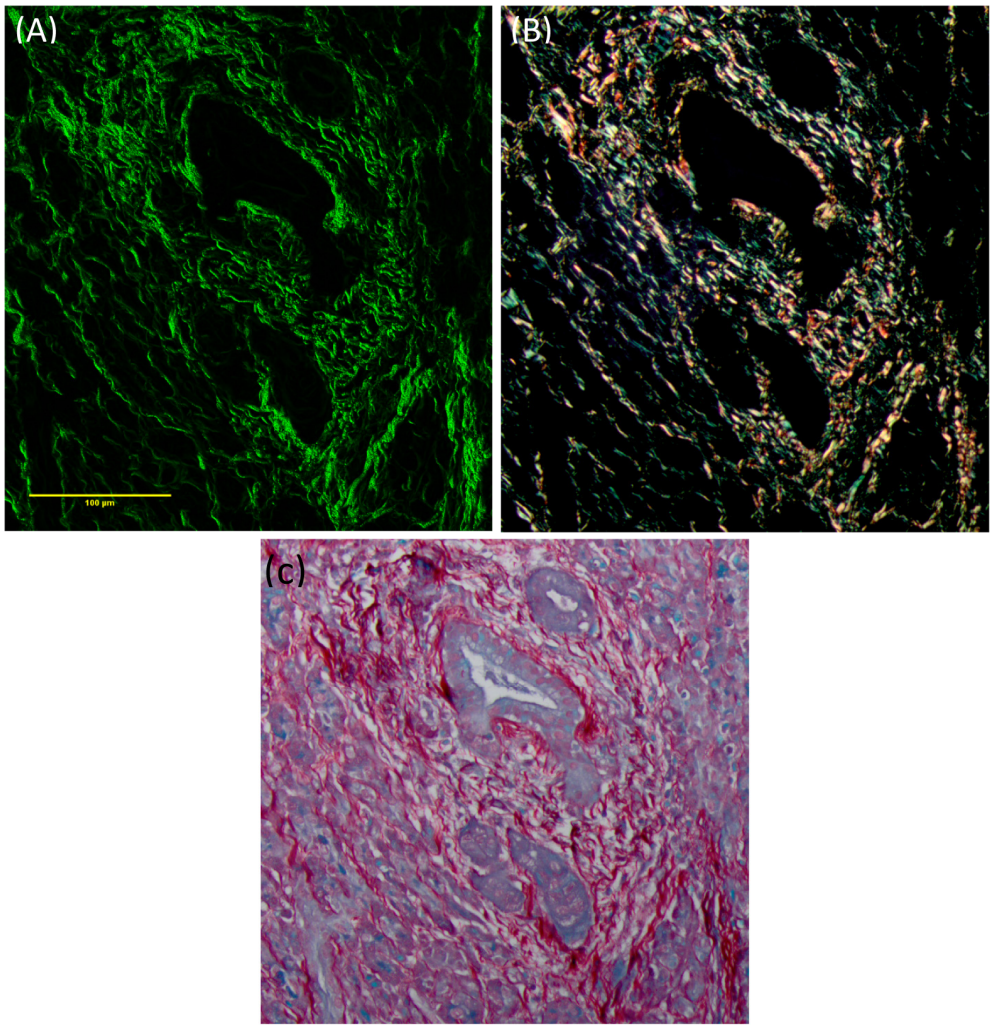

Fig. 3. Collagen imaging using (A) PolScope, (B) traditional polarized microscope and (B) bright field image of a picrosirius stained pancreatic cancer tissue. The collagen fibers are shown in green and red in (A) and (C), respectively, and the collagen fibers have different colors including orange-red for thick ones and green-yellow for thin ones.

Figure 4 shows a region from a breast tissue imaged using SHG and LC-PolScope systems, Fig. 4(A) and 4(B). The CT-FIRE fiber detection results and also three selected ROIs are represented in Fig. 4(C) and 4(D).

Biomedical Optics EXPRESS

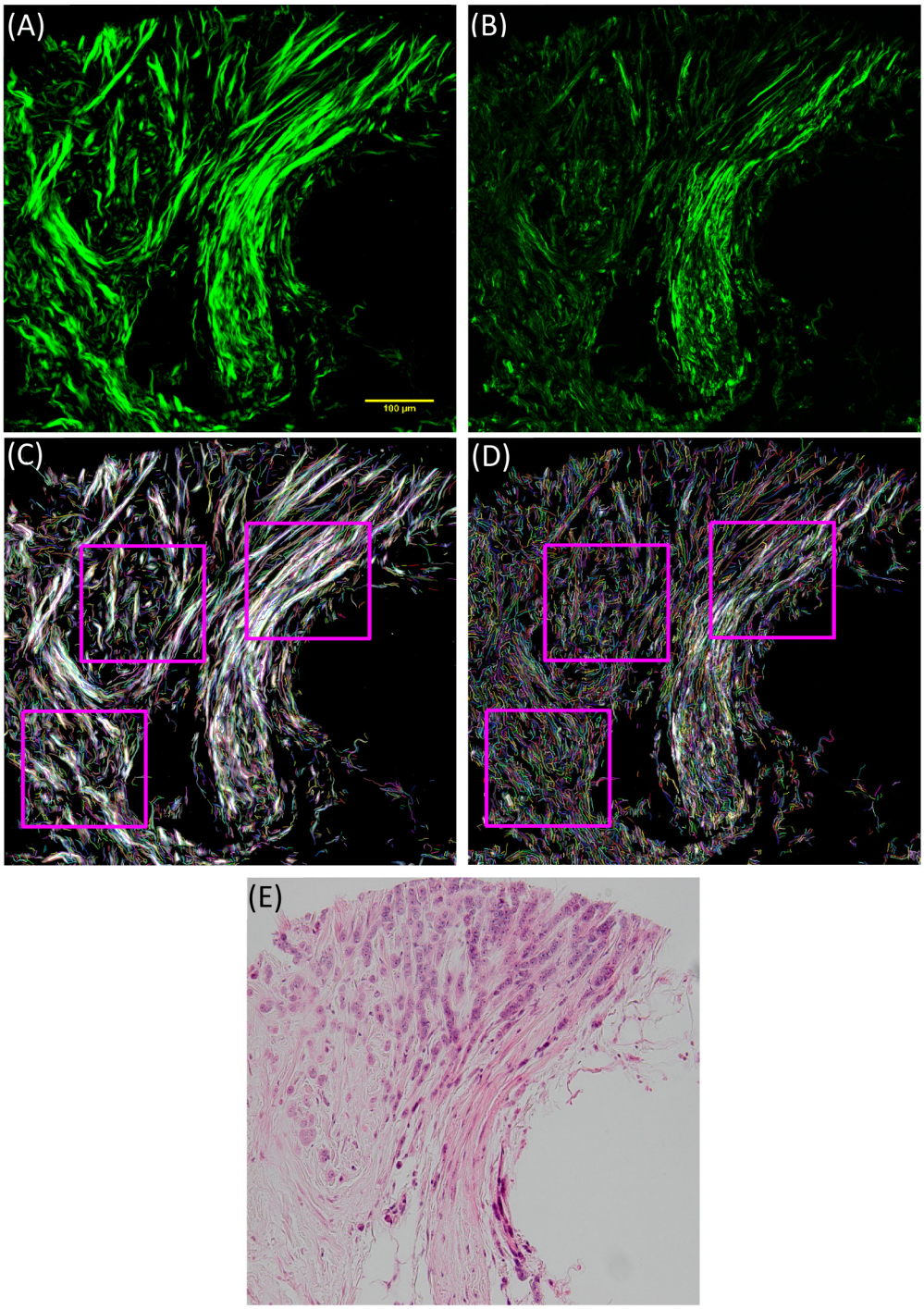

Fig. 4. Comparison of LC-PolScope and SHG imaging on breast tissue slides. Breast tissue sample imaged with PolScope (A) and SHG (B). The CT-FIRE fiber detection results and ROI selection for PolScope (C) and SHG (D). Part (E) shows the bright field image of the same region. To be noted, CT-FIRE was run on the thresholded PolScope image as displayed in (A). The fibers in (C) and (D) are displayed in randomly selected false colors for visualization purpose. Brighter regions in (A) indicate thick or closely packed fibers.

Biomedical Optics EXPRESS

Figure 5 shows a region from a pancreatic tissue imaged using SHG and LC-PolScope systems, Fig. 5(A) and 5(B). The CT-FIRE fiber detection results and also three selected ROIs are represented in Fig. 5(C) and 5(D).

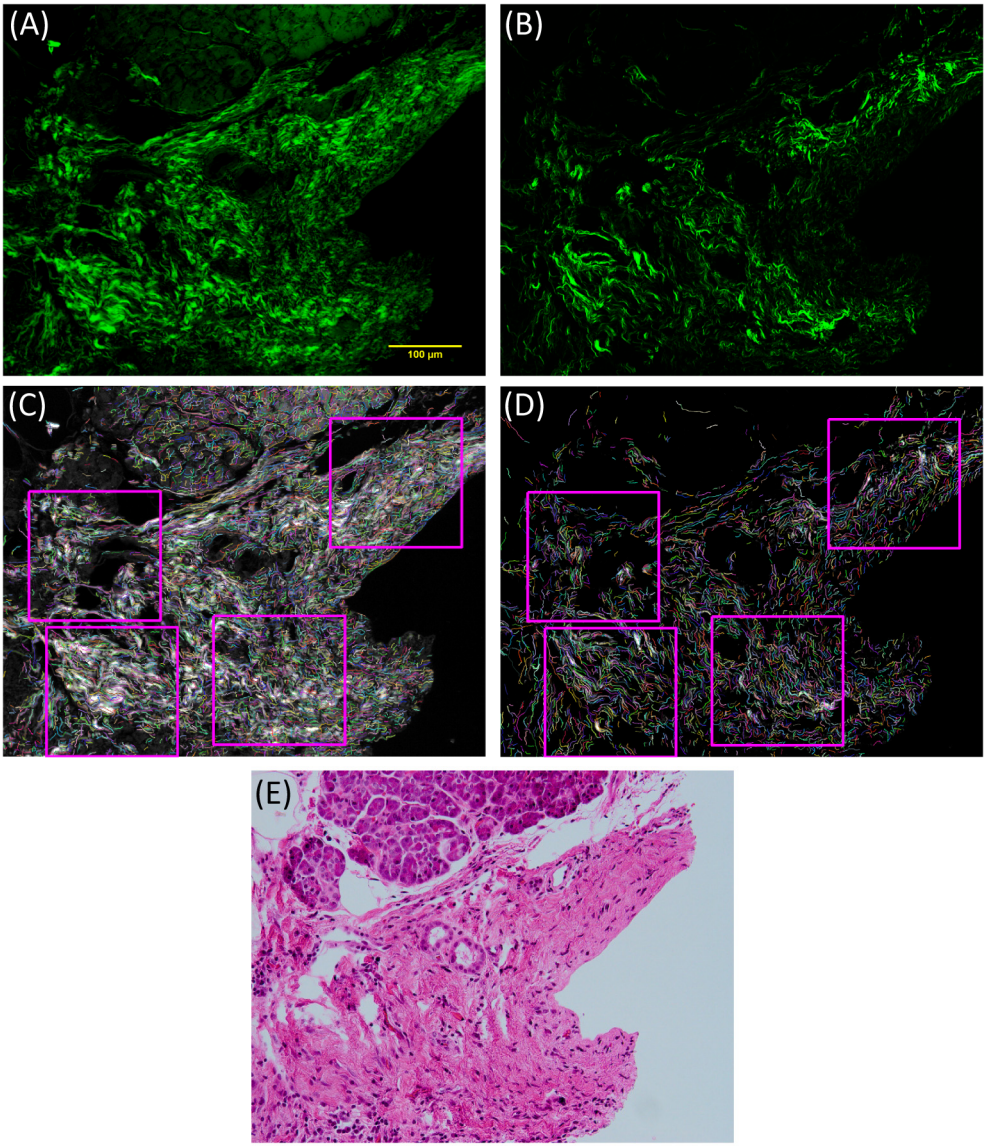

Fig. 5. Comparison of PolScope and SHG imaging on pancreatic tissue slides. Pancreatic tissue sample imaged with PolScope (A) and SHG (B). The CT-FIRE fiber detection results and ROI selection for PolScope (C) and SHG (D). Part (E) shows the bright field image of the same region. The fibers in (C) and (D) are displayed in randomly selected false colors for visualization purpose. Brighter regions in (A) indicate thick or closely packed fibers.

Table 1 summarizes the results for orientation and alignment for breast and pancreatic cancer. The mean, standard deviation, median, and range for 39 ROIs from 10 breast cancer patients and 135 ROIs from 24 pancreatic cancer patients are listed.

Biomedical Optics EXPRESS

Table 1. Orientation and alignment summary results for breast and pancreatic cancer

Tissue sample	Measurement	Modality	Mean (SD)	Median (Range)
Breast (39 ROIs from 10 Patients)	Orientation	SHG	83.4 (39.2)	86.9 (1.2-171.4)
		PolScope	85.7 (55.7)	87.5 (1.4-178.5)
	Alignment	SHG	0.41 (0.16)	0.45 (0.05-0.66)
		PolScope	0.42 (0.17)	0.42 (0.1-0.82)
Pancreatic (135 ROIs from 24 patients)	Orientation	SHG	98.2 (46.3)	109 (0.2-179.8)
		PolScope	98.6 (53)	109 (3.5-178)
	Alignment	SHG	0.49 (0.19)	0.5 (0.09-0.85)
		PolScope	0.54 (0.21)	0.56 (0.01-0.89)

The Bland-Altman plots of orientation and alignment for breast cancer ROIs are plotted in Fig. 6. Bland-Altman plot shows the difference between two measurements of the same parameter vs. the average of these values [41]. Red dotted lines show the mean and the green lines show the (mean ± 1.96 STD), which is called the 95% confidence interval (CI).

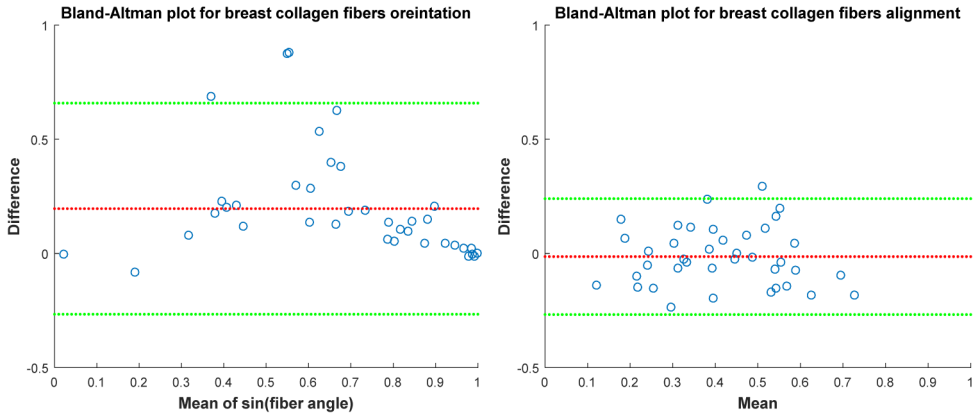

Fig. 6. Bland-Altman plot for orientation (left) and alignment (right) in breast cancer. Red dotted lines show the mean values 0.1959 and –0.0141 for the orientation and alignment. Green lines show the 95% confidence interval.

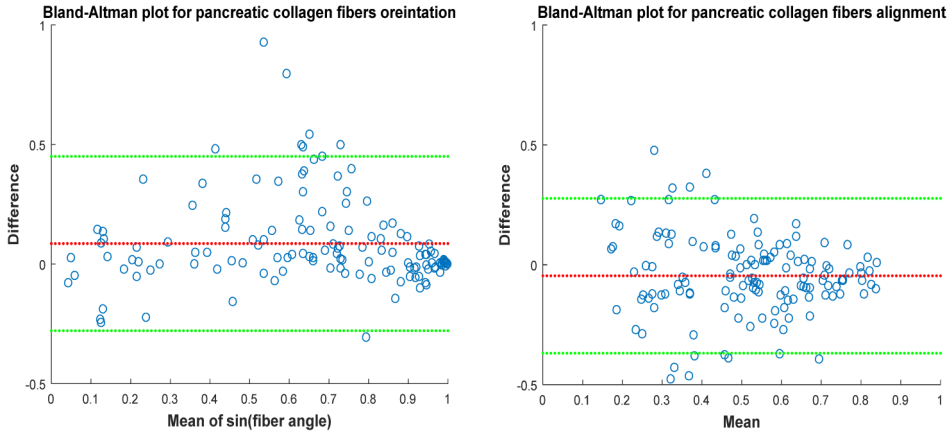

Fig. 7. Bland-Altman plot for orientation (left) and alignment (right) in pancreatic cancer. Red dotted lines show the mean values 0.0858 and –0.0458 for the orientation and alignment. Green lines show the 95% confidence interval.

Biomedical Optics EXPRESS

10 patients with breast cancer were used for imaging with SHG and LC-PolScope. Orientation and alignment in breast and pancreatic cancer were measured in 2-4 ROI for each patient. The estimated correlation for orientation as measured by SHG and PolScope in breast cancer was 0.68, and the estimated correlation was 0.69 for alignment. The agreement between SHG and PolScope for orientation and alignment in breast cancer is good. 24 patients had pancreatic cancer that was evaluated using SHG and PolScope. The estimated correlation for orientation as measured by SHG and PolScope in pancreatic cancer was 0.80, and the estimated correlation for alignment was 0.65. The agreement between SHG and PolScope for orientation in pancreatic cancer is excellent, and the agreement for alignment is good.

4. Discussion

Growing research in histopathological collagen analysis demands cheaper, quicker and less sample preparation and complexity due to the high cost, relatively slow collection and complexity of SHG instrumentation. On the other hand, pathological staining involves more process and possible changes in workflow. The need for a more compact, easily accessible and clinically applicable method led us toward using an alternative collagen imaging method for thin sectioned tissue samples. PolScope is a highly sensitive tool for birefringence measurement. Thus it should be able to readily detect fibrillar collagen as it is a highly ordered molecule and one of the most birefringent proteins in the body. Traditional polarized microscopes usually use picrosirius staining which intensifies the dichroism of collagen fibers reported to be 700% by Junqeira et al [16] and 5-6 times by [42]. We observed 10-15 times increase in collagen dichroism enhancement in breast and pancreatic cancer tissues in our experiments using PolScope. This discrepancy is probably because of the different tissue types and staining methods. Although we believe because of higher sensitivity of PolScope compared to traditional microscopes, it might be a better method for further investigation of birefringence/dichroism enhancement. There is no published evidence that H&E staining elevates the dichroism/birefringence of the tissue. Our preliminary tests confirmed no significant change in dichroism/birefringence of H&E stained tissue compared to unstained samples. For this reason we decided to use H&E stained samples since it's easier to find the same region on different microscopes. Another advantage of using H&E is that it increases the utility for pathologists and biologists, as H&E is the gold standard histopathology labeling method for research and clinical applications. Traditional polarized light microscopy relies on rotating the stage for identifying birefringent or dichroic samples, which is not always the best solution, because it can introduce undesired displacement. This has been solved in PolScope by using a liquid crystal to rotate or change the polarization state electronically without the need to move any part. Hence, all the images taken with different polarization are perfectly registered. Unlike traditional polarized microscope in which the compensator converts retardance values to a color, using the subtraction of a specific wavelength from white light [43], PolScope can measure this parameter precisely.

Using collagen I antibody stained slides, as the gold standard method, helped us verify that PolScope can visualize all the type I collagen fibers (Fig. 2), which is one of the abundant collagen fiber types in these pancreatic and breast samples. Although there are other types of molecules in the body that show birefringence properties such as lipid bilayers of the cell plasma membrane, mitotic spindle fibers, actin filament bundles, and etc [43], collagen fibers, due to their thickness and highly aligned molecular bonds, usually show much stronger birefringence which makes it the dominant value to set the birefringence ceiling that is being mapped to the image highest intensity. This way the other birefringent parts of the cell will have much lower brightness and can be easily removed by intensity thresholding. This is important as future applications of Polscope to other tissue types will need to differentiate collagen signal from other birefringent signals. This is a noted advantage still of SHG in that the signal is selective for collagen.

Biomedical Optics EXPRESS

PolScope images are captured using a lower NA (o.4) objective compared to SHG (1.25). So visualizing thinner fibers demanded using high lamp power, which in turn results in saturating very thick or closely packed bundle of fibers. However, orientation and alignment would not change.

Picrosirius red staining collagen is still one of the most popular methods collagen imaging for pathological practice and research. Although PolScope doesn't need any staining for collagen imaging, it still outperforms traditional polarized microscopy of picrosirius stained samples in terms of fiber orientation dependency and sensitivity to smaller fibers (Fig. 3). Since unlike traditional polarized microscopy, PolScope visualizes all the fibers in all directions with the same intensity, the discontinuities in the fibers path are much less and fiber tracking and quantification is more accurate.

Since in this study the pathological information of the patients was not the concern, the ROIs were selected mostly from collagen rich regions that show different levels of alignment visually. The alignment and orientation comparison results for breast and pancreatic cancer show that PolScope can be used as a very cheap, less bulky, and user friendly alternative for collagen imaging in thin sectioned samples. For the statistical analysis we used a linear mixture model, which estimates the correlation between two measurements of the same parameter measured with different methods. According to the interpretation method from [44] the guidelines for interpretation are as follows: less than 0.40 - poor; 0.40-0.59 fair; 0.60-0.74 good; 0.75-1.00 excellent. The agreement between SHG and PolScope for orientation (0.68) and alignment (0.69) in breast cancer is good and the agreement between SHG and PolScope for orientation in pancreatic cancer is excellent (0.80), and the agreement for alignment is good (0.65). Although the results show that PolScope can be utilized for collagen network organization analysis, there are different sources that contribute to the deviation from complete correlation. Some of these reasons are: 1) Unlike SHG imaging LC-Polscope is not specific to fibrillar collagen. LC-Polscope can detect other birefringent parts of tissue such as cell membrane, nuclei membrane, actin filament, mitotic spindle, etc. 2) The two systems (SHG and PolScope) have completely different imaging physics and they need their specific optical parts like the objective lenses, which require different coating and NA for each modality. Multiphoton microscopy objectives are designed to provide high transmission over a wide wavelength range for transmitting stimulation and emission signals. Whereas polarized microscopy objectives are designed for less polarization distortion. Since high NA can distort light polarization, polarization microscopy objectives are chosen to be low NA for blocking any unwanted beam. So the higher NA objective selected for SHG imaging (1.25NA Vs 0.4 NA for PolScope) will result in higher resolution and aid in visualizing more of thinner fibers with different orientations.

3) CT-FIRE recognizes the fiber image discontinuities and very curvy fibers as several fibers with different orientations.

In this study we used CT-FIRE for fiber detection and CurveAlign for alignment calculation. As we mentioned earlier there are other parts of the tissues and cells that are birefringent but their retardance value is much smaller than collagen. This can be seen in the top part of Fig. 5(A). This will allow us to successfully eliminate those regions by thresholding when we are just interested in collagen imaging. The thresholding can be performed on the image itself. Here we used the thresholding option in CT-FIRE and the threshold value was set to 30 in all the 8 bit images. Considering the retardance ceiling value set to 15 nm, this threshold value corresponds to ~1.7 nm for the retardance.

This was a preliminary study to investigate the PolScope possibilities for collagen visualization and we will proceed to utilize other PolScope possibilities such as slow axis orientation measurements for investigating collagen fiber structure and the effect of different disease such as cancer on this parameter. We are also testing the sensitivity of PolScope to different collagen types, specially collagen type IV, to figure out which types can be

Biomedical Optics EXPRESS

visualized, as well as looking for a way to distinguish between different collagen types, based on their optical properties.

5. Conclusion

In this study we showed when looking at the orientation and alignment of a collagen network in thin sections, PolScope can be used as a practical and viable alternative to SHG and staining. Using PolScope as a cost effective, simple and compact system would be desirable in clinical trials or by pathologists in their workflows.

Funding

Morgridge Institute for Research and National Institutes of Health (NIH) (U54DK104310 and R01GM114274); The University of Wisconsin Carbone Cancer Center Cancer Center Biocore and Histology core (UWCCC) (P30 CA014520).

Acknowledgement

The authors gratefully acknowledge illuminating discussions on statistical analysis with Jens Eickhoff, Department of Biostatistics & Medical Informatics at UW-Madison.

Disclosures

The authors declare that there are no conflicts of interest related to this article.